

# Buffeting response control of a long span cable-stayed bridge during construction using semi-active tuned liquid column dampers

K. M. Shum<sup>†</sup> and Y. L. Xu<sup>‡</sup>

*Department of Civil and Structural Engineering, The Hong Kong Polytechnic University,  
Hung Hom, Kowloon, Hong Kong, China*

W. H. Guo<sup>††</sup>

*School of Civil Engineering and Architecture, Central South University,  
Changsha, Hunan 410075, P.R. China*

*(Received May 2, 2005, Accepted May 9, 2006)*

**Abstract.** The frequency of a traditional tuned liquid column damper (TLCD) depends solely on the length of liquid column, which imposes certain restrictions on its application to long span cable-stayed bridges during construction. The configuration of a cable-stayed bridge varies from different construction stages and so do its natural frequencies. It is thus difficult to apply TLCD with a fixed configuration to the bridge during construction or it is not economical to design a series of TLCD with different liquid lengths to suit for various construction stages. Semi-active tuned liquid column damper (SATLCD) with adaptive frequency tuning capacity is studied in this paper for buffeting response control of a long span cable-stayed bridge during construction. The frequency of SATLCD can be adjusted by active control of air pressures inside the air chamber at the two ends of the container. The performance of SATLCD for suppressing combined lateral and torsional vibration of a real long span cable-stayed bridge during construction stage is numerically investigated using a finite element-based approach. The finite element model of SATLCD is also developed and incorporated into the finite element model of the bridge for predicting buffeting response of the coupled SATLCD-bridge system in the time domain. The investigations show that with a fixed container configuration, the SATLCD with adaptive frequency tuning can effectively reduce buffeting response of the bridge during various construction stages.

**Keywords:** semi-active tuned liquid column damper; cantilever construction; lateral and torsional vibration; wind excitation; pressure; parametric studies.

---

## 1. Introduction

It is efficient and economic to construct long span cable-stayed bridges by using one-sided

---

<sup>†</sup> PhD, Research Associate, Email: [kmslum2005@gmail.com](mailto:kmslum2005@gmail.com)

<sup>‡</sup> PhD, Chair Professor, Email: [ceylxu@polyu.edu.hk](mailto:ceylxu@polyu.edu.hk)

<sup>††</sup> PhD, Professor

free-cantilevering approach and/or double free-cantilevering approach. Although long span cable-stayed bridges are more stable in its final condition, they are often vulnerable to wind excitation during construction stage. If it is located at a wind-prone region, much attention is required for controlling buffeting response of an incomplete bridge, as bending stiffness of the bridge deck during construction is much smaller than that of the complete bridge in lateral, vertical and torsional directions. Besides, buffeting forces on the incomplete bridge also differ from those on the complete bridge. It is thus necessary to explore the way of minimizing disturbance of excessive deck vibration to erection work and ensuring the safety of the bridge under high winds.

There are several ways to reduce wind-induced vibration of long span cable-stayed bridges during construction. Installing temporary cables on bridge girders is one of the most common methods to stiffen the bridge deck during construction. However, it has been reported that in some circumstances the use of temporary tie-down may be subjected to a high construction cost of anchor block and a risk of ship collision during storm (Virlogeux 1992). Utilizing mechanical control devices to supplement damping capacity of bridge structure can be an alternative solution for reducing wind-induced vibration. To ease erection work and avoid interaction with ship navigation, tuned mass dampers (TMD) were installed on the Normandy Bridge during its construction for suppressing the lateral vibration of two cantilevering bridge decks. Conti, *et al.* (1996) demonstrated that the lateral buffeting response of the decks during construction could be reduced by at least 35% after the installation of the TMD. Takeda, *et al.* (1998) studied active mass dampers (AMD) for controlling the vertical buffeting response of concrete cable-stayed bridges during cantilever construction. They showed that the structural damping of the bridge was enhanced significantly by the implementation of AMD and thereby the vibration of bridge was reduced considerably. However, the configuration of a long span cable-stayed bridge varies from different construction stages and so do its natural frequencies. Thus, it is difficult to change and tune the frequency of a passive mass damper or liquid damper to the varying-structural frequency of the bridge during the entire construction period.

In consideration of the features of a long span cable-stayed bridge during construction, semi-active tuned liquid column dampers (SATLCD) with frequency adaptability are investigated in this paper to suppress combined lateral and torsional vibration of a long span cable-stayed bridge under different stages of cantilever construction. Semi-active tuned liquid column dampers (SATLCD) have two control capacities, the control of its natural frequency and the control of liquid motion within the tolerable limit. The desired control force acting on the liquid column is provided by regulating the pressure difference inside the air chambers at the two ends of the container. Five different construction stages of a real long span cable-stayed bridge are selected as a case study for the evaluation of SATLCD performance and adaptability. Wind forces acting on the bridge, including both buffeting and self-excited forces, are generated in the time domain using computer simulation techniques in addition to the measured aerodynamic coefficients and flutter derivatives. The finite element model of SATLCD is also developed and incorporated into the finite element model of the bridge and a computer program is correspondingly written for predicting buffeting response of the coupled SATLCD-bridge system. The performance of SATLCD for the suppression of lateral and torsional vibration of the real long span cable-stayed bridge during construction is evaluated through parametric studies. The key parameters investigated include mass ratio, head loss coefficient, mean wind speed and cantilever length.

## 2. Modeling of cable-stayed bridge and liquid damper

### 2.1. Modeling of cable-stayed bridge

A long span cable-stayed bridge under construction can be represented by a three-dimensional finite element model using different types of finite elements such as beam element, cable element, plate element and solid element. In this study, stay cables are modeled as cable element whose elastic modulus is modified by the Ernst's formula in order to include the sag effect of cable due to its self-weight. Three-dimensional Timoshenko beam elements are used to model bridge towers and deck. The mass matrix, stiffness matrix and force vector of the bridge are obtained by the use of traditional finite element method (Xu, *et al.* 1997). The geometric nonlinear stiffness due to tension forces in the cables and axial forces in the bridge deck and towers is also considered in the modeling of the bridge. The damping matrix of the bridge, which is assumed to be the Rayleigh damping, can be expressed as a combination of the mass and stiffness matrices.

$$[C_b] = \alpha_b[M_b] + \beta_b[K_b] \tag{1}$$

where  $[M_b]$ ,  $[C_b]$ , and  $[K_b]$  are the mass, damping and stiffness matrices of the bridge, respectively;  $\alpha_b$  and  $\beta_b$  are the Rayleigh damping factors, which can be evaluated if the first two modal damping ratios and natural frequencies of the bridge are known.

### 2.2. Modeling of liquid damper

The SATLCD with frequency adaptability capacity is a U-shaped container with uniform cross-sectional area (see Fig. 1). Liquid is filled into its container, and two chambers are filled with compressed air of static pressure  $P_o$ . The control force is applied on the liquid in terms of a net external pressure between the two air chambers. The net pressure is regulated by the displacement and velocity of the liquid column in a prescribed way so that the target natural frequency and damping of liquid motion inside the SATLCD can be easily achieved. The net pressure between the two air chambers, sensed by pressure transducers, is forced to follow or track the desired pressure determined by a computer in accordance with a given control algorithm and a targeted frequency. Any deviation from the desired pressure is fed back to the computer to take corrective action to

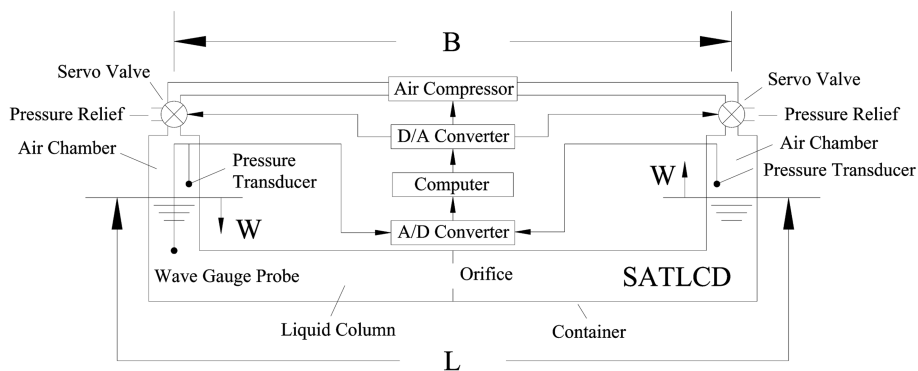


Fig. 1 Schematic diagram of semi-active tuned liquid column dampers

adjust the servo valves. Thus, the control system is continually monitoring and correcting pressure deviation to maintain the desired pressure acting on the liquid column and the targeted frequency. In practice, a number of SATLCD are required for reducing vibration of a bridge. The control force is composed of two parts: one is displacement feedback force for the control of liquid oscillation frequency and the other is velocity feedback force for the control of liquid damping. The displacement feedback control force  $u_{1k}(t)$  in the  $k$ th SATLCD is given by

$$u_{1k}(t) = S_k \cdot W_k(t) \quad (2)$$

where  $S_k$  is the constant displacement feedback gain of the  $k$ th SATLCD; and  $W_k(t)$  is the displacement of the liquid column. The direction of the control force  $u_{1k}(t)$  is in the same (opposite) direction as the liquid displacement  $W_k(t)$  when the constant displacement feedback gain is positive (negative). With the control force expressed by Eq. (2), the circular natural frequency,  $\omega_k$ , of liquid motion in the  $k$ th SATLCD can be determined by

$$\omega_k^2 = \frac{2g}{L_k} + \frac{S_k}{\rho_w A_k L_k} \quad (3)$$

where  $g$  is the acceleration due to gravity;  $L_k$  is the length of the  $k$ th SATLCD;  $A_k$  is the cross-sectional area of the  $k$ th SATLCD; and  $\rho_w$  is the density of liquid inside the  $k$ th SATLCD. For a targeted frequency of the liquid damper, it can easily be seen from Eq. (3) that the liquid column length of the  $k$ th SATLCD is given by

$$L_k = \frac{2g}{\omega_k^2} + \frac{S_k}{\rho_w A_k \omega_k^2} \quad (4)$$

Clearly, the liquid column length can be increased or decreased by adjusting the constant displacement feedback gain while keeping its frequency unchanged. The SATLCD is therefore more flexible than the traditional TLCD in which  $S_k$  is equal to zero and there is no way for changing the liquid column length if the frequency is given. Once the frequency and length of the liquid column are decided, the required constant displacement feedback gain of the  $k$ th SATLCD can be determined by

$$S_k = m_k \left[ \omega_k^2 - \frac{2g}{L_k} \right] \quad (5)$$

where  $m_k$  is the mass of the  $k$ th SATLCD. The malfunction of SATLCD may result from its excessive liquid motion when the bridge is subjected to high winds. An on-off control algorithm is therefore employed to make sure the liquid motion inside the SATLCD is within the tolerable limit. This velocity feedback control force is regulated by manipulating the pressure in accordance with the on-off control strategy as follows:

$$u_{2k}(t) = \begin{cases} \frac{1}{2} \rho_w A_k \delta_m |\dot{W}_k| \dot{W}_k & \text{if } (W_k > K_p \cdot W_a) \text{ and } (\dot{W}_k \cdot W_k > 0) \\ 0 & \text{otherwise} \end{cases} \quad (6)$$

where  $W_a$  is the tolerable liquid displacement of the  $k$ th SATLCD (see Eq. 14);  $K_p$  is an adjusting factor less than or equal to 1;  $\delta_m$  is the head loss coefficient for providing sufficient damping to the  $k$ th SATLCD and it depends on  $K_p W_a$ . Since the space inside the bridge deck is not large enough to

provide sufficiently long vertical column, the adoption of this particular control strategy (Eq. (6)) is to avoid the overflow of liquid inside the damper in particular for the bridge under high wind speed. The nonlinear damping force selected is to correlate this additional damping force with the passive damping force in term of head loss coefficient for easy manipulation. The control force is so selected that the additional damping is provided to the liquid when the liquid is continually increased and beyond certain level ( $K_p \cdot W_a$ ). The factor  $K_p$  decides how the liquid displacement is close to the tolerable liquid displacement and when the additional damping control force should be added to the damper. In other words, larger value of the factor  $K_p$  would require a large value of  $\delta_m$  to suppress the liquid motion as it gets closer to the tolerable liquid displacement than the case with a smaller value of  $K_p$ . The total control force acting on the  $k$ th SATLCD is then the sum of the control force,  $u_{1k}$ , based on the feedback of liquid displacement and the control force,  $u_{2k}$ , based on the feedback of liquid velocity.

$$u_k = \begin{cases} S_k W_k + \frac{1}{2} \rho_w A_k \delta_m |\dot{W}_k| \dot{W}_k & \text{if } (W_k > K_p \cdot W_a) \text{ and } (\dot{W}_k \cdot W_k > 0) \\ S_k W_k & \text{otherwise} \end{cases} \quad (7)$$

The desired control force acting on the liquid column can be provided by regulating the air pressure in the right chamber with respect to the air pressure in the left chamber to obtain a net pressure  $P_k(t)$ . The relation between the net pressure and the control force can be expressed as

$$u_k = P_k(t) \cdot A_k \quad (8)$$

The net pressure  $P_k(t)$  in the  $k$ th SATLCD can be obtained from Eq. (7) as

$$P_k(t) = \begin{cases} \frac{S_k W_k}{A_k} + \frac{1}{2} \rho_w \delta_m |\dot{W}_k| \dot{W}_k & \text{if } (W_k > K_p \cdot W_a) \text{ and } (\dot{W}_k \cdot W_k > 0) \\ \frac{S_k W_k}{A_k} & \text{otherwise} \end{cases} \quad (9)$$

Inside the  $k$ th SATLCD, the air pressure in the left chamber  $P_L$  and in the right chamber  $P_R$  is then determined, respectively, by

$$P_L = P_o - \frac{P_k(t)}{2}, \quad P_R = P_o + \frac{P_k(t)}{2} \quad (10)$$

Investigation on the performance of SATLCD interacting with a simple structure with simplified dynamic loads has been carried out by the authors (Shum and Xu 2005). It has been shown that the maximum pressure required for SATLCD is about 100 kPa for the structure under white noise excitation. The availability of an air compressor to meet the requirement has been checked with the compressor suppliers. The maximum operating pressure of air compressor can be up to 900 kPa. The corresponding air flow required would be 254 liter/min and the energy required is about 1500 W. It may also be worthwhile to mention that passively pressurized TLCD has been successfully applied to suppress ship oscillation in lateral direction (Kagawa, *et al.* 1989). A passively pressurized TLCD uses the differential pressure between two closed air chambers to control the oscillation of liquid motion but it is of the passive nature rather than the semi-active control presented in this paper. The

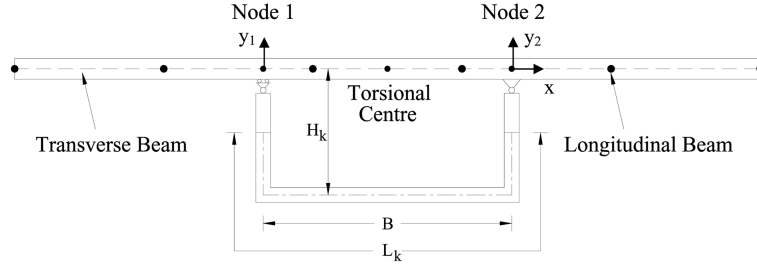


Fig. 2 Connections between bridge deck and liquid damper

experimental results of using differential pressure between two chambers to actively control a hydraulic damper can be found in Jelali and Kroll (2003). These results make the proposed SATLCD prospective to be implemented in real civil engineering structures.

To consider the interaction between semi-active liquid column dampers and a long span cable-stayed bridge under wind excitation, it is expedient to derive the finite element model of the liquid dampers so that it can be incorporated into the finite element model of the bridge. Let us consider a total of  $n_T$  units of SATLCD installed below the torsional centre of the bridge deck and at the locations where vibration amplitudes of the bridge in the lateral and torsional directions are the largest. The SATLCD units are connected to the transverse beams of the bridge deck by roller supports and simply supports as shown in Fig. 2. Two additional nodes, namely node 1 and node 2, are generated at the positions where the SATLCD units are connected to the bridge. These two additional nodes reflect the motion of the SATLCD units interacted with the motion of the bridge. From a view point of practical use, the distance between the two vertical columns  $B$  is the same for all SATLCD units. The axial deformation of the transverse beam between the two supports is assumed to be negligible and hence the lateral displacement of the SATLCD units is taken as  $x$  and the torsional displacement of the SATLCD units is then determined by

$$\theta = \frac{y_2 - y_1}{B} \quad (11)$$

where  $x$  is the lateral displacement of the node 2;  $y_1$  and  $y_2$  are the vertical displacements of the node 1 and 2, respectively. The Lagrangian of all SATLCD units can be expressed as follows:

$$L_d = \sum_{k=1}^n \left[ \frac{1}{2} m_k \dot{W}_k^2 + \frac{1}{2} m_k \dot{x}^2 + \frac{1}{2} I_k \dot{\theta}^2 + m_k \alpha_k \dot{W}_k \dot{x} + G_k \dot{W}_k \dot{\theta} + m_k \bar{H}_k \dot{x} \dot{\theta} \right. \\ \left. + m_k g \bar{H}_k \cos \theta - m_k g \alpha_k W_k \sin \theta - \frac{m_k g}{L_k} W_k^2 \cos \theta - \frac{S_k}{2} W_k^2 \right] \quad (12)$$

where  $I_k$  is the second moment of the liquid mass inside the  $k$ th SATLCD;  $\alpha_k$  is the liquid length ratio  $= B_k/L_k$ ;  $\bar{H}_k$  is the distance from the mass center of liquid inside the  $k$ th SATLCD to the torsional (elastic) center of the bridge deck;  $G_k$  is the first moment of the liquid mass in the  $k$ th SATLCD; and the last term in Eq. (12) is the potential energy of liquid due to the control force  $u_{1k}$  in the  $k$ th SATLCD. In Eq. (12), the effect of vertical acceleration of the bridge deck on the liquid motion is neglected because it is relatively small compared with the acceleration due to gravity. The expressions for  $I_k$ ,  $\bar{H}_k$ , and  $G_k$  are given as follows:

$$\begin{aligned}
 I_k &= m_k \left( \alpha_k \left[ H_k^2 + \frac{B_k^2}{12} \right] + (1 - \alpha_k) \left[ H_k^2 + \frac{B_k^2}{4} - \frac{H_k(L_k - B_k)}{2} + \frac{(L_k - B_k)^2}{12} \right] \right) \\
 \bar{H}_k &= H_k - \frac{(L_k - B_k)^2}{4L_k} \\
 G_k &= m_k \alpha_k \left( H_k + \frac{L_k - B_k}{2} \right)
 \end{aligned} \tag{13}$$

where  $H_k$  is the vertical distance between the centerline of the horizontal part of the container and the torsional center of the bridge deck. Eq. (12) is subjected to the condition that the liquid should be fully retained in the horizontal part of the SATLCD and thus the following equation should always be satisfied.

$$W_k \leq \frac{L_k - B_k}{2} - \frac{d_k}{2} = W_a \tag{14}$$

where  $d_k$  is the thickness of the liquid column in the  $k$ th SATLCD; and  $W_a$  is defined as the tolerable liquid displacement of the  $k$ th SATLCD. The entries of mass matrix  $m_{ij}$  and stiffness matrix  $k_{ij}$  of the SATLCD (damper element) can be determined by

$$m_{ij} = \frac{\partial}{\partial \dot{q}_j} \left( \frac{\partial L_d}{\partial \dot{q}_i} \right), \quad k_{ij} = -\frac{\partial}{\partial q_j} \left( \frac{\partial L_d}{\partial q_i} \right) \tag{15}$$

$$[q]^T = [x \quad y_1 \quad y_2 \quad W_1 \quad \dots \quad W_N] \tag{16}$$

After some manipulations, the mass matrix of the damper element,  $[M]$ , and the stiffness matrix of the damper element,  $[K]$ , can be written as

$$[M] = \begin{bmatrix} M_{11} & M_{12} \\ M_{12}^T & M_{22} \end{bmatrix} \text{ and } [K] = \begin{bmatrix} K_{11} & K_{12} \\ K_{12}^T & K_{22} \end{bmatrix} \tag{17}$$

where

$$M_{11} = \frac{1}{B^2} \begin{bmatrix} m_d B^2 & -mB & -mB \\ -mB & I_d & -I_d \\ -mB & -I_d & I_d \end{bmatrix} \quad M_{12} = \begin{bmatrix} m_1 \alpha_1 & m_2 \alpha_2 & \dots & m_N \alpha_N \\ -\frac{G_1}{B} & -\frac{G_2}{B} & \dots & -\frac{G_N}{B} \\ \frac{G_1}{B} & \frac{G_2}{B} & \dots & \frac{G_N}{B} \end{bmatrix} \tag{18}$$

$$M_{22} = \text{diag}(m_1, m_2, \dots, m_N) \tag{19}$$

$$K_{11} = \frac{m\mathcal{G}}{B^2} \begin{bmatrix} 0 & 0 & 0 \\ 0 & 1 & -1 \\ 0 & -1 & 1 \end{bmatrix} \quad K_{12} = \frac{\mathcal{G}}{B} \begin{bmatrix} 0 & 0 & \dots & 0 \\ -m_1 \alpha_1 & -m_2 \alpha_2 & \dots & -m_N \alpha_N \\ m_1 \alpha_1 & m_2 \alpha_2 & \dots & m_N \alpha_N \end{bmatrix} \tag{20}$$

$$K_{22} = \text{diag}(m_1 \omega_1^2, m_2 \omega_2^2, \dots, m_N \omega_N^2) \quad (21)$$

where  $m_d$  is the total liquid mass of all SATLCD units;  $I_d$  is the total second moment of the liquid mass of all SATLCD units with respect to the torsional center of the bridge deck; and  $m = \sum_{k=1}^N m_k \bar{H}_k$ .

The vertical motion of liquid inside the liquid column has been taken into consideration by including the restoring force of liquid due to gravitational force in vertical direction. The vertical inertia effect of liquid mass in the global finite element model has also been considered by modeling it as lumped masses at the corresponding node.

### 3. Equation of motion of coupled system

The finite element model of the coupled SATLCD-bridge system can be constituted by combining the finite element model of the bridge with the finite element model of the SATLCD. The equation of motion of the coupled SATLCD-bridge system can be obtained correspondingly.

$$\begin{bmatrix} M_b + M_{bbd} & M_{bd} \\ M_{bd} & M_d \end{bmatrix} \begin{Bmatrix} \ddot{v}_b \\ \ddot{v}_w \end{Bmatrix} + \begin{bmatrix} C_b & \mathbf{0} \\ \mathbf{0} & C_d \end{bmatrix} \begin{Bmatrix} \dot{v}_b \\ \dot{v}_w \end{Bmatrix} + \begin{bmatrix} K_b + K_{bbd} & K_{bd} \\ K_{bd} & K_d \end{bmatrix} \begin{Bmatrix} v_b \\ v_w \end{Bmatrix} = \begin{Bmatrix} P_{buff} + P_{se} \\ \mathbf{0} \end{Bmatrix} \quad (22)$$

where  $\{v_b\}$ ,  $\{\dot{v}_b\}$ , and  $\{\ddot{v}_b\}$  are the dynamic displacement, velocity, and acceleration vectors of the bridge, respectively. The matrix  $[v_w]_{n_T \times 1}$  represents the liquid displacement vector of the  $n_T$  units of SATLCD. The matrix  $[M_{bbd}]$  is associated with the inertial forces of the liquid due to the global motion of liquid columns and it is obtained by assembling the liquid damper matrix  $[M_{11}]$ . The matrix  $[M_d]$  corresponds to the inertia forces of the liquid due to the relative motions of liquid columns to the containers and it is obtained by assembling the liquid damper matrix  $[M_{22}]$ . The matrix  $[M_{bd}]$  indicates that the structural motion and the liquid motion are coupled by inertia effects of the liquid and it is obtained by assembling the liquid damper matrix  $[M_{12}]$ . The matrices  $[K_{bbd}]$  and  $[K_{bd}]$  are related to the restoring forces resulting from gravitational effects of the liquid and they are obtained by assembling the liquid damper matrix  $[K_{11}]$  and  $[K_{12}]$  respectively. The matrix  $[K_d]$  corresponds to the liquid restoring forces due to the liquid elevation difference between the two vertical columns and it is obtained by assembling the liquid damper matrix  $[K_{22}]$ . The matrix  $[C_d]$  represents the nonlinear damping forces resulting from the damper orifice and it is given by

$$[C_d] = \text{diag}\left(\frac{1}{2}\rho_w A_1 \delta_1 |\dot{W}_1|, \frac{1}{2}\rho_w A_2 \delta_2 |\dot{W}_2|, \dots, \frac{1}{2}\rho_w A_{n_T} \delta_{n_T} |\dot{W}_{n_T}|\right) \quad (23)$$

where  $\delta_k$  is the head loss coefficient of the  $k$ th SATLCD. In Eq. (22),  $\{P_{buff}\}$  and  $\{P_{se}\}$  are the buffeting force vector and the self-excited force vector of the bridge, respectively, which are assembled from the buffeting forces and self-excited forces acting on all the nodes of the bridge. It will be noted in the subsequent section that the self-excited forces at a particular time instant are dependent on the motion of the bridge at that time instant. Iterations are generally required at each time step to determine the self-excited forces until the prescribed convergence is satisfied.

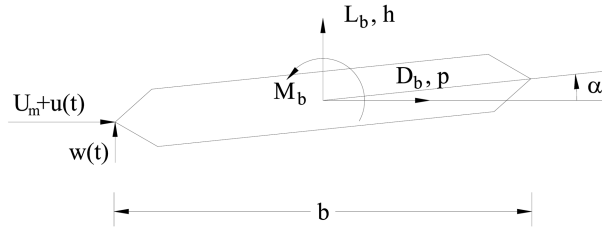


Fig. 3 Aerodynamic forces of bridge deck

#### 4. Wind forces on cable-stayed bridge

The aerodynamic forces acting on the bridge can be resolved into buffeting forces and self-excited forces. The buffeting forces are due to incident wind turbulences acting on the bridge and the self-excited forces are due to the interaction between the bridge motion and the wind.

##### 4.1. Buffeting forces

The buffeting forces are caused by wind turbulences  $u$  and  $w$  in the alongwind and vertical wind directions. The buffeting forces per unit length as shown in Fig. 3 can be determined by the following expressions:

$$D_b(t) = \frac{1}{2} \rho_a U_m^2 b \left[ C_D \frac{2u(t)}{U_m} + C'_D \frac{w(t)}{U_m} \right] \quad (24a)$$

$$L_b(t) = \frac{1}{2} \rho_a U_m^2 b \left[ C_L \frac{2u(t)}{U_m} + (C'_L + C_D) \frac{w(t)}{U_m} \right] \quad (24b)$$

$$M_b(t) = -\frac{1}{2} \rho_a U_m^2 b^2 \left[ C_M \frac{2u(t)}{U_m} + C'_M \frac{w(t)}{U_m} \right] \quad (24c)$$

where  $U_m$  is the mean wind speed;  $D_b(t)$ ,  $L_b(t)$ , and  $M_b(t)$  are the buffeting drag, lift and moment, respectively, on the bridge deck per unit span length;  $\rho_a$  is the air density;  $b$  is the deck width;  $C_L$ ,  $C_D$ , and  $C_M$  are the lift, drag and moment coefficients obtained from wind tunnel tests of the bridge deck section model;  $C'_L$ ,  $C'_D$ , and  $C'_M$  are the slopes of  $C_L$ ,  $C_D$  and  $C_M$  at the angle  $\alpha$ , respectively;  $\alpha$  is the angle of attack of normal incident wind referring to the horizontal plane of the bridge deck; and  $u(t)$  and  $w(t)$  are the fluctuating wind speed components in the alongwind and vertical wind direction, respectively. The aerodynamic admittance function is considered as unity in this study. A fast spectral representation method proposed by Cao, *et al.* (2000), which is based on the spectral representation method developed by Yang (1972, 1973) and Shinozuka, *et al.* (1972), is adopted here for the digital simulation of stochastic wind velocity field along the bridge deck.

##### 4.2. Self-excited forces

The self-excited forces on the bridge deck are caused by interaction between the wind and the

bridge motion. The bridge system taps the energy from wind flow by means of its deflection and the time derivatives of deflection. The vibration amplitude of the bridge system may be increased to a catastrophic level if the energy of motion extracted from the flow exceeds the energy dissipated by the bridge system. The self-excited forces per unit span length can be expressed in terms of convolution integrals as follows (Lin and Yang 1983):

$$D_{se}(t) = \rho_a U_m^2 \int_{-\infty}^t [I_{Dh}(t-\tau)h(\tau) + I_{Dp}(t-\tau)p(\tau) + I_{D\alpha}(t-\tau)\theta(\tau)]d\tau \quad (25a)$$

$$L_{se}(t) = \rho_a U_m^2 \int_{-\infty}^t [I_{Lh}(t-\tau)h(\tau) + I_{Lp}(t-\tau)p(\tau) + I_{L\alpha}(t-\tau)\theta(\tau)]d\tau \quad (25b)$$

$$M_{se}(t) = \rho_a U_m^2 \int_{-\infty}^t [I_{Mh}(t-\tau)h(\tau) + I_{Mp}(t-\tau)p(\tau) + I_{M\alpha}(t-\tau)\theta(\tau)]d\tau \quad (25c)$$

where  $h$ ,  $p$ , and  $\theta$  are the vertical, lateral, and torsional dynamic displacements of the bridge deck at a given position;  $I_0$  represents the impulse response function of the self-excited force, in which the subscripts indicate the corresponding force components. The impulse response function can be obtained from wind tunnel test results (Scanlan 1978) together with the rational function approximation techniques (Chen, *et al.* 2000). Then, for example, by using Eq. (25b), the self-excited lift induced by the vertical displacement of the bridge deck, the first term in Eq. (25b), can be expressed as

$$L_{seh}(t) = \frac{1}{2}\rho_a U_m^2 \left[ C_1 h(t) + C_2 \frac{B}{U_m} \dot{h}(t) + C_3 \frac{B}{U_m^2} \ddot{h}(t) + \sum_{k=1}^n \phi_k(t) \right] \quad (26)$$

where  $C_1$ ,  $C_2$ ,  $C_3$ ,  $C_{k+3}$ , and  $d_k$  ( $d_k \geq 0$ ;  $k=1,2,\dots,n$ ) are the frequency independent coefficients of the rational functions. The first and second terms in Eq. (26) represent the aerodynamic stiffness and the aerodynamic damping which are determined by the linear and nonlinear least squares methods using the measured flutter derivatives at different reduced frequencies; and  $\phi_k(t)$  ( $k=1,2,\dots,n$ ) are new variables that satisfy the following equations.

$$\dot{\phi}_k(t) = -\frac{d_k U_m}{B} \phi_k(t) + C_{k+3} \dot{h}(t) \quad (k=1,2,\dots,n) \quad (27)$$

The derivation procedure can be applied to other self-excited force components to obtain similar formulations, which are omitted here for the sake of brevity.

## 5. Response of bridge during construction without control

### 5.1. A long span cable-stayed bridge

A real long span cable-stayed bridge is selected as a case study for the evaluation of SATLCD performance and adaptability. The selected bridge is a triple tower cable-stayed bridge with an overall length of 1177 m and the two main spans of 448 m and 475 m and the two side spans of 127 m each (see Fig. 4). Five different construction stages of the concerned bridge are selected (see Fig. 5). The bridge deck consists of two carriage-way structures and the overall width of the bridge deck is 42.8 m. The central pylon reaches a height of 200 m above sea level with the end towers having heights of 163 m and 172 m above sea level respectively. The three bridge pylons are all

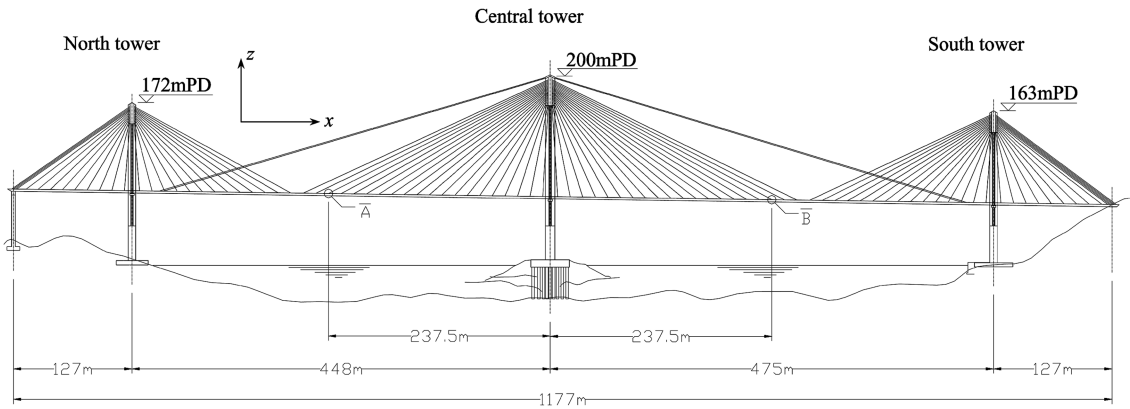


Fig. 4 Configuration of long span cable-stayed bridge used in case study

single leg concrete pylons. Two large steel tower heads, each weighing some 170 tons, are installed at the top of each tower from which 384 stay cables in four planes radiate downwards to support the bridge deck at 13.5 m intervals. The tower are further stabilized by transverse cables running from the tower head to the cross struts and the section of tower below deck level. The central tower is further stabilized longitudinally with eight longitudinal stay cables. The bridge deck is separated into two carriageway structures and each carriageway structure is formed by two longitudinal steel plate girders with steel beams spanning transversely between them at 4.5 m centers. Each carriageway structure is represented by a three-girder model consisting of one central girder and two side girders connected by transverse links.

Fig. 5 shows that the bridge under construction stage 1 is divided into three parts and they are erected simultaneously. Each part of the bridge deck is free at its two ends and its transverse

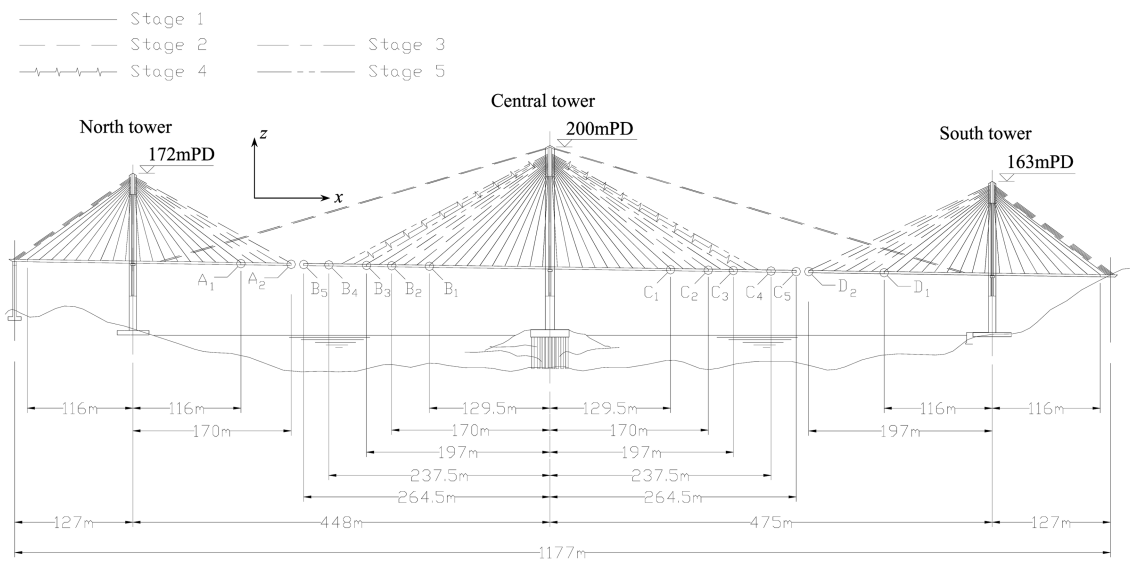


Fig. 5 Configuration of long span cable-stayed bridge under five different construction stages

restraint is provided by the tower only. The deck-to-tower connections offer longitudinal and lateral displacement restraints with essentially completely free rotation about all three axes together with free vertical displacement. The span length of all incomplete bridge decks becomes longer at stage 2 and the central pylon is stabilized by the longitudinal stabilizing cables. The incomplete bridge deck at two side spans is fixed transversely and vertically at one end. The span of the incomplete bridge deck at the central tower is increased gradually from stage 3 to stage 5 and the bridge is almost completed under construction stage 5. The bridge is represented by a three dimensional dynamic finite element model, which takes into account the geometric nonlinear effect of axial forces on the bending of the bridge deck and the tension of cables. The first two modal damping ratios of the bridge are taken as 0.8%.

### 5.2. Simulation of wind force

The wind velocity field along the bridge girders in either alongwind direction or vertical wind direction is simulated by ninety-six ( $n$ ) fluctuating wind velocity time histories at ninety-six different points evenly distributed along the bridge deck with an interval distance of 13.5 m. The power spectral density (PSD) functions of the alongwind  $u$  and vertical wind  $w$  are given by the von Kármán spectra as follows.

$$\frac{fS_{u_i u_i}(f)}{\sigma_u^2} = \frac{4Z_u}{(1 + 70.78Z_u^2)^{5/6}}; \quad \frac{fS_{w_r w_r}(f)}{\sigma_w^2} = \frac{2(1 + 188.8Z_w^2)Z_w}{(1 + 70.78Z_w^2)^{11/6}}; \quad Z_r = \frac{fL_r^y}{U_m} \quad (28)$$

where  $L_r^y$  is the integral scale of the  $r$  wind component in the alongwind direction;  $f$  is the frequency in Hz;  $\sigma_u$  and  $\sigma_w$  are the standard deviations of wind turbulent in the alongwind and vertical wind directions. The cross spectral density (CSD) function between points  $i$  and  $j$  are given by

$$S_{r_i r_j}(f) = \sqrt{S_{r_i r_i}(f)S_{r_j r_j}(f)} \exp\left(-\lambda \frac{\eta_r}{2\pi}\right); \quad \eta_r = \frac{0.747|x_i - x_j|}{L_r^x} \sqrt{1 + 70.78\left(\frac{fL_r^x}{U_m}\right)^2} \quad (29)$$

In this study, the turbulent intensity at the bridge deck level in the alongwind direction ( $I_u$ ) and in the vertical direction ( $I_w$ ) are 0.10 and 0.05, respectively. The integral scales of alongwind turbulence in the alongwind direction and the bridge longitudinal direction ( $L_u^y$ ,  $L_u^x$ ) are of 80 m and those of vertical wind turbulence in the alongwind direction and the bridge longitudinal direction ( $L_w^y$ ,  $L_w^x$ ) are of 40 m. The parameter  $\lambda$  in Eq. (29) is taken as 8 as a constant value. The upper cutoff frequency ( $f_{up}$ ) is taken as 10 Hz and the dividing number of frequency ( $N$ ) is  $2^{14}$ . The corresponding frequency interval ( $\Delta f$ ) and the time interval of wind velocity histories ( $\Delta t$ ) are 0.000305 Hz and 0.05 s respectively. The drag, lift and moment coefficients of the bridge deck measured from the wind tunnel tests are 0.103, 0.134, and  $-0.011$  respectively, at the zero wind angle of attack with respect to the deck width of 42.8 m (Tan 1999). The first derivatives of the drag, lift, and moment coefficients ( $C'_D$ ,  $C'_L$ ,  $C'_M$ ) with respect to wind angle at the zero wind angle of attack are 0.00, 5.25, and 1.06, respectively. In the simulation of the self-excited forces, only the flutter derivatives ( $H_1^*$ ,  $H_4^*$ ,  $A_2^*$ , and  $A_3^*$ ) of the concerned cable-stayed bridge are available from wind tunnel tests (Choi and Brownjohn 1998, Tan 1999). For the flutter derivatives in the lateral direction, they are considered by the quasi-steady theory as follows:

$$P_1^* = -\frac{C_D}{k}; \quad P_4^* = 0 \tag{30}$$

where  $k$  is the reduced frequency.

### 5.3. Dynamic characteristics of bridge

The dynamic characteristics of the bridge are first determined for its natural frequencies and mode shapes. The generalized mass and mass moment of inertia of the bridge deck are determined by

$$M_{Lj}^* = \int_{deck} \bar{m}(x) \psi_{Lj}^2(x) dx; \quad M_{Vj}^* = \int_{deck} \bar{m}(x) \psi_{Vj}^2(x) dx; \quad I_{Tj}^* = \int_{deck} \bar{I}(x) \psi_{Tj}^2(x) dx \tag{31}$$

where  $x$  is the coordinate along the bridge longitudinal axis;  $\bar{m}(x)$  and  $\bar{I}(x)$  are the mass and mass moment of inertia of the bridge deck per unit length;  $\psi_{Lj}(x)$ ,  $\psi_{Vj}(x)$ , and  $\psi_{Tj}(x)$  are respectively the  $j$ th normalised lateral, vertical and torsional mode shape of the bridge deck.

The eigenvalue analysis of the finite element model of the bridge shows that the largest amplitude in the first mode shape of the bridge deck during construction occurs at the tip of the cantilever in the lateral, vertical and torsional direction, respectively. The first lateral, vertical and torsional frequencies of the bridge at the side span increase significantly when one of its ends is fixed. The natural frequencies of the bridge at the central tower part are summarized in Tables 1 to 3 for construction stages from one to five. It is observed that the lateral frequency of the bridge at the central tower part does not vary as much as that in the vertical and torsional direction but it is much lower than that in the other two directions. The vertical frequency of the bridge at the central tower part is increased from construction stage 1 to stage 2 and is decreased gradually from construction stage 2 to stage 5. The torsional frequency of the bridge deck is decreased from construction stage 1 to stage 5. The first lateral mode shape of the bridge deck at the central tower part is in weather-

Table 1 First lateral frequency and generalized mass of the double cantilever deck at the central tower

Stage	Frequency (Hz)	Generalized mass ( $M_L^*$ )/kg
1	0.04677	$2.48160 \times 10^6$
2	0.04606	$3.12910 \times 10^6$
3	0.04555	$4.11101 \times 10^6$
4	0.04492	$4.24095 \times 10^6$
5	0.04505	$4.68761 \times 10^6$

Table 2 First vertical frequency and generalized mass of the double cantilever deck at the central tower

Stage	Frequency (Hz)	Generalized mass ( $M_V^*$ )/kg
1	0.17602	$2.00085 \times 10^6$
2	0.22302	$2.90739 \times 10^6$
3	0.18148	$2.40548 \times 10^6$
4	0.16140	$2.65769 \times 10^6$
5	0.13683	$2.30176 \times 10^6$

Table 3 First torsional frequency and generalized mass moment of the double cantilever deck at the central tower

Stage	Frequency (Hz)	Generalized mass moment of inertia ( $I_T^*$ ) / $\text{kgm}^2$
1	0.93165	$1.54822 \times 10^8$
2	0.77281	$1.44241 \times 10^8$
3	0.38114	$1.28881 \times 10^8$
4	0.37469	$1.52893 \times 10^8$
5	0.27757	$2.21612 \times 10^8$

vane motion. The geometric stiffness of cables provides the lateral stiffness to the bridge deck. As the deck length increases, the cable stiffness increases almost proportionally to the increase in mass, leading to small variation in the first lateral frequency of the bridge at the central tower part. The increase in vertical frequency of the bridge from construction stage 1 to stage 2 can be attributed to the effect of longitudinal stabilizing cables. The first vertical mode shape of the bridge deck at the central tower part involves the bending of the central tower. The longitudinal stabilizing cables indeed stiffen the central tower and hence the stiffness of the tower is increased after the installation of the longitudinal stabilizing cables. As the deck length is further increased, vertical or torsional frequency of the bridge deck is decreased.

#### 5.4. Buffeting response of bridge at different construction stages

To have a better understanding of wind-induced vibration of the bridge, the buffeting responses of the concerned bridge at five different construction stages are computed at a mean wind speed of 20 m/s, and their corresponding standard deviation displacement responses are displayed in Fig. 6. The points A and D represent the locations at the tips of the cantilevers of the two side bridge decks. The points B and C represent the locations at the tips of the double cantilever of the bridge deck at the central tower part. For the cantilevers of the two side bridge decks under construction stage 1, excessive vibration is observed in the lateral direction. However, they are decreased significantly when the side deck is fixed on the ground at one of its ends. For the double cantilever deck at the central tower part, excessive lateral vibration of the double cantilever deck is observed for the five construction stages. For the vertical and torsional displacements of the double cantilever, they increase significantly as the cantilever deck length is increased. This is because the bending stiffness of the double cantilever deck in the vertical and torsional directions is decreased with the increasing cantilever length. The small difference in torsional response between points B and C could be attributed to the different lengths of the two main spans and hence the unsymmetrical profile of bridge deck. Besides, the tension forces of the cables on the two sides are also different in order to meet the required geometry (vertical profile) of the deck. It is clear that the lateral and torsional vibrations of double cantilever deck is more serious than that of the two side bridge decks for the concerned five construction stages. To control the buffeting response of the bridge deck with variation in natural frequency during five construction stages, the SATLCD with frequency adaptability is a potential control device. Hence, the application of SATLCD in reducing the lateral and torsional vibration of the double cantilever deck at the central tower part will be studied in the next section with focus on its performance and adaptability during various construction stages of the bridge. Due to the nature of SATLCD, the vertical vibration reduction of the bridge cannot be considered.

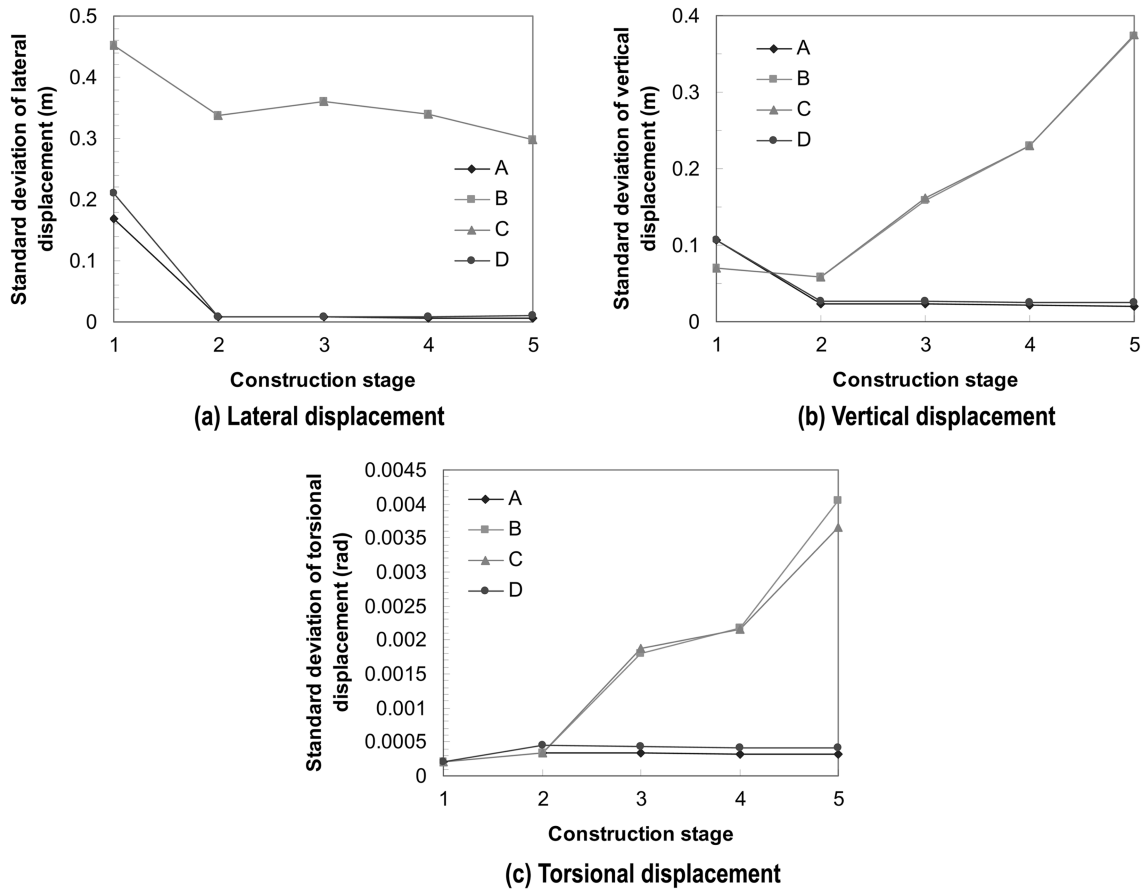


Fig. 6 Buffeting response of bridge deck during various construction stages at mean wind speed of 20 m/s

Displayed in Fig. 7 are the time histories of the deck displacement responses in lateral, vertical and torsional directions at point B of the double cantilever deck at construction stage 5 under the mean wind speed of 20 m/s. To further understand the vibration nature of the bridge deck, the spectrum analysis is also performed using the given time histories of deck displacements. The resulting PSD functions are shown in Fig. 8. The PSD functions of lateral and torsional displacement of the bridge deck at point B show that both lateral and torsional displacements of the bridge deck are dominated by one single peak at the frequency around 0.045 Hz and 0.28 Hz, respectively. For the vertical displacement, the PSD function at point B has two peaks at the frequency around 0.135 and 0.195 Hz. The peak frequencies appearing in the PSD functions match quite well with the computed natural frequencies obtained from the dynamic characteristics analysis (see Tables 1 to 3).

### 6. Performance of SATLCD

In general, the mass ratio  $\mu_{tj}$  for the SATLCD tuned to the  $j$ th mode of lateral vibration of the bridge is defined as

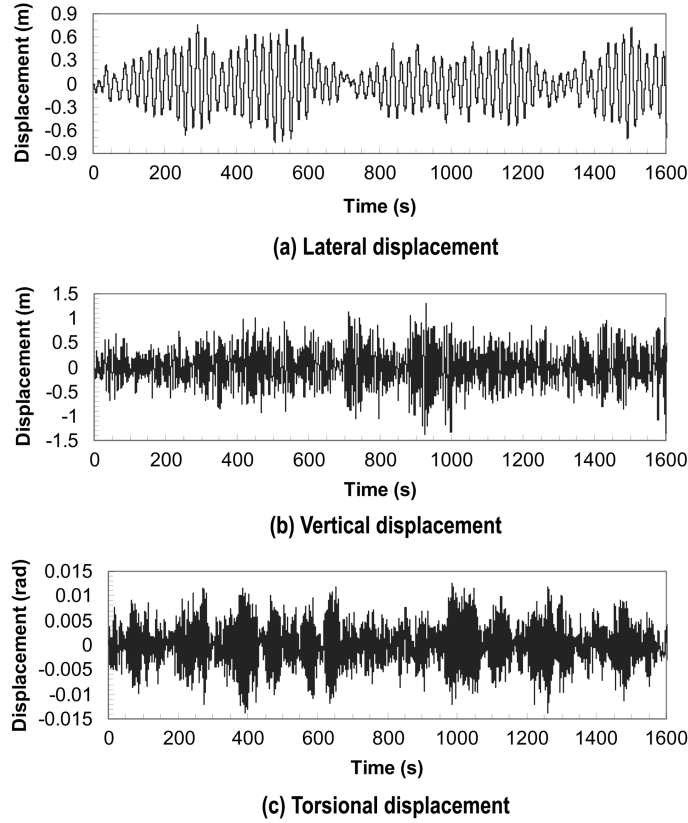


Fig. 7 Time histories of displacements of the bridge at point B subjected to turbulent wind ( $U_m = 20.0$  m/s)

$$\mu_{Lj} = \frac{m_{Lj}}{M_{Lj}^*} \quad (32)$$

The mass ratio  $\mu_{Tj}$  for the SATLCD tuned to the  $j$ th mode of torsional vibration of the bridge is defined as

$$\mu_{Tj} = \frac{m_{Tj} I_j}{I_{Tj}^*} \quad (33)$$

where  $m_{Lj}$  is the mass of SATLCD tuned to the  $j$ th lateral vibration mode of the bridge;  $m_{Tj}$  is the mass of SATLCD tuned to the  $j$ th torsional vibration mode of the bridge;  $I_j$  is the second moment of SATLCD per unit mass tuned to the  $j$ th torsional mode of vibration. The total liquid mass of all SATLCD units ( $m_d$ ) is determined by

$$m_d = \sum_{j=1}^{n_L} m_{Lj} + \sum_{j=1}^{n_T} m_{Tj} = \mu m_s \quad (34)$$

where  $n_L$  is the number of lateral modes of vibration to be controlled;  $n_T$  is the number of torsional modes of vibration to be controlled; and  $\mu$  is the mass ratio of the total liquid mass to the mass of the bridge deck ( $m_s$ ). The performance of SATLCD is assessed in terms of the response ratio  $R$ ,

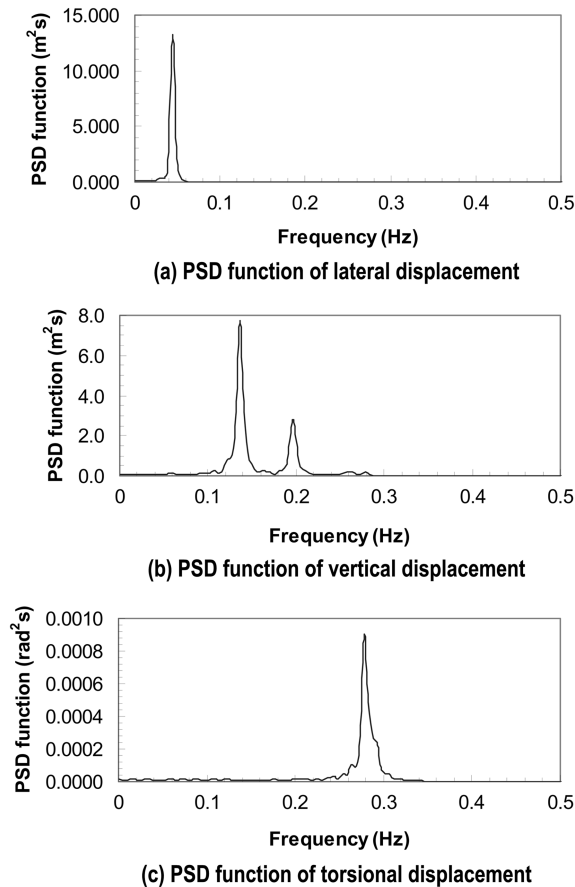


Fig. 8 PSD functions of displacements of the bridge at point B subjected to turbulent wind ( $U_m = 20.0$  m/s)

which is defined as the ratio of the structural response with control to the structure response without control. The mean wind speed considered in this study is 20 m/s unless it is otherwise specified. As described in the previous section, the lateral and torsional vibration of the concerned long span bridge consists of only one major frequency component. Two SATLCD units with one tuned to the first lateral frequency of the bridge and the other tuned to the first torsional frequency of the bridge are installed at each end of the double cantilever deck. From a view point of practical use, the geometric configurations of all SATLCD units are taken to be the same. In this study, the liquid column length is selected to be 21.5 m and the thickness of liquid column of 1.1 m.

### 6.1. Effect of mass ratio

The effects of the mass ratio  $\mu$  on the performance of SATLCD in reducing lateral and torsional displacement of the double cantilever deck at the central tower part under construction stage 5 are depicted in Fig. 9. The total mass of the double cantilever deck under construction stage 5 is  $1.34215 \times 10^7$  kg. The parameters of the SATLCD used herein are  $H = 6.5$  m,  $\alpha = 0.6$ ,  $\delta_1 = 5$ ,  $\delta_2 = 105$ , and  $\mu_l = \mu_t$ . The parameters of SATLCD tuned to the first lateral and torsional frequency of

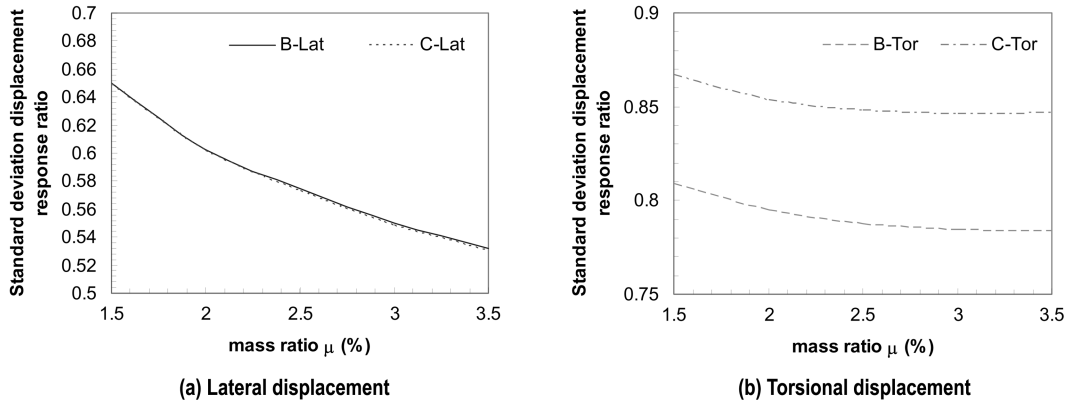


Fig. 9 Effect of mass ratio on the performance of SATLCD

the double cantilever bridge deck are denoted by the subscripts 1 and 2 respectively. The dropping of the subscript in some damper parameters implies that these parameters are the same for the two dampers. To achieve different mass ratios of the SATLCD, the width of the liquid column, which is in the direction perpendicular to the elevation of the damper, is changed accordingly. It can be seen from Fig. 9 that the lateral displacement at points B and C are reduced significantly with the increase in mass ratio but the reduction of the torsional displacement at points B and C is less sensitive to the mass ratio. There is almost no change in torsional displacement response ratio at points B and C when the mass ratio is beyond a value of 2.7%. The SATLCD with a mass ratio of 2.7% is thus selected for further parametric studies on the control of buffeting response of the double cantilever deck. For this mass ratio, the decrease in torsional displacement can achieve about 15% and the decrease in the lateral displacement is about 40%. The performance of SATLCD in reducing lateral displacement at points B and C are almost the same and the reduction of torsional displacement at point B is slightly better than that at point C.

## 6.2. Effect of head loss coefficient

The effects of head loss coefficient on the performance of SATLCD in reducing the lateral and torsional displacement responses of the double cantilever deck under construction stage 5 are depicted in Fig. 10. The corresponding pressure inside the air chamber is also plotted in the figure. The parameters of the SATLCD used herein are  $H=6.5$  m,  $\alpha=0.6$ ,  $\mu=0.027$ , and  $\mu_l=\mu_t$ . The two SATLCD units at each end of the double cantilever are assumed to take the same value of head loss coefficient for the same motion. It can be seen from Fig. 10 that the effectiveness of SATLCD is affected by head loss coefficient and the optimal head-loss coefficients exist for the maximum reduction of lateral and torsional displacement responses. The head loss coefficient for achieving the maximum reduction in lateral displacement response is much smaller than that for achieving the maximum reduction in torsional displacement response. The optimal head loss coefficients for achieving the maximum reduction in lateral or torsional displacement at point B are almost same as that at point C. It can also be seen that for torsional displacement reduction, the performance of SATLCD is less sensitive to the head loss coefficient. The performance would not be deteriorated much even the head loss coefficient slightly offsets from the optimal value. Fig. 10 also indicates that

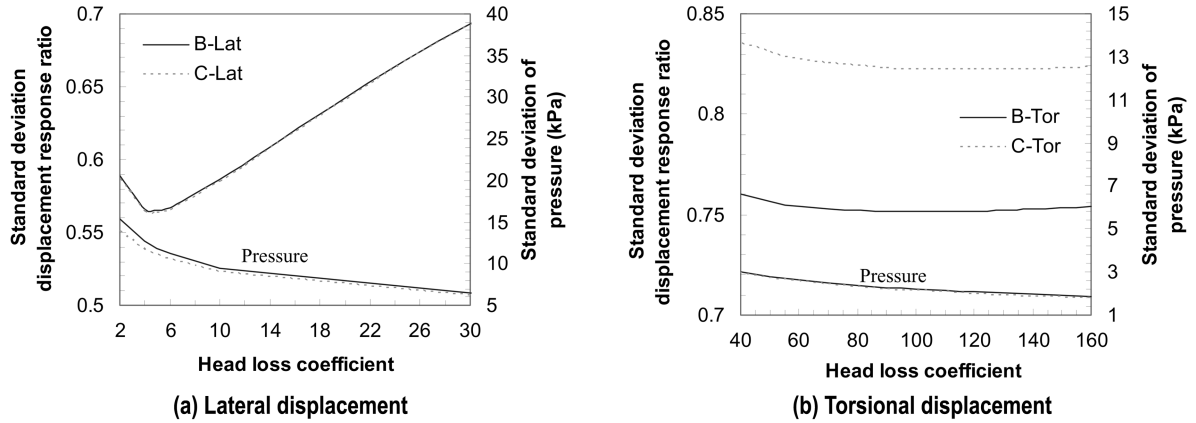


Fig. 10 Effect of head loss coefficient

the pressure required for feedback control force is decreased with the increasing head loss coefficient.

### 6.3. Effect of mean wind speed

The application of liquid column dampers to the cable-stayed bridge during construction aims at minimizing the disturbances to erection work due to excessive deck vibration and ensuring the safety of the bridge deck under high winds. It is thus important to investigate the performance of SATLCD in reducing buffeting response of the bridge deck under different mean wind speeds. To have a reasonable assessment of the performance of SATLCD in reducing buffeting response of the bridge, head loss coefficient is taken as a variable to find its optimal value for achieving the maximum reduction of standard deviation displacement response ratio at a given construction stage. Other parameters of the SATLCD used herein are  $H=6.5$  m,  $\alpha=0.6$ ,  $\mu=0.027$ , and  $\mu_l=\mu_T$ . To avoid the malfunction of SATLCD due to its excessive liquid motion under high mean wind speed, additional control force is provided to control the liquid displacement within the tolerable limit when the liquid is continuously increased and beyond 75% (i.e.  $K_p=0.75$ ) of tolerable liquid displacement. With the choice of  $K_p$  equal to 0.75 and the tolerable liquid displacement ( $W_a$ ) equal to 3.75 m, the liquid motion at which the control force  $u_{2k}$  becomes active is 2.81 m, and the head loss coefficient  $\delta_m$  is selected to be 200 to provide sufficient damping force to the liquid inside SATLCD. The values of  $K_p$  and  $\delta_m$  have only a little influence on the optimal parameters of the SATLCD as the inclusion of  $u_{2k}$  merely provides an additional damping force to the damper other than (or very little) to the bridge. The use of a sufficient large value of head loss coefficient could avoid the liquid overflow but at the cost of significant deterioration of damper performance in reducing lateral displacement response. For instance, if the value of  $K_p$  is less than 0.75, the additional damping force will be increased and the liquid displacement will be restricted to a level that is smaller than 2.81 m. The energy dissipation of the damper and the bridge vibration reduction will then become smaller. Besides, the smaller value of  $K_p$  would require more energy to activate and maintain the control force  $u_{2k}$ . Therefore, the value of  $K_p$  should be selected with the full consideration of the liquid overflow, the control effectiveness and the control energy.

Fig. 11 shows the displacement response ratios of the SATLCD-bridge system under different mean wind speeds. The corresponding pressure inside the air chamber is also plotted in the figure.

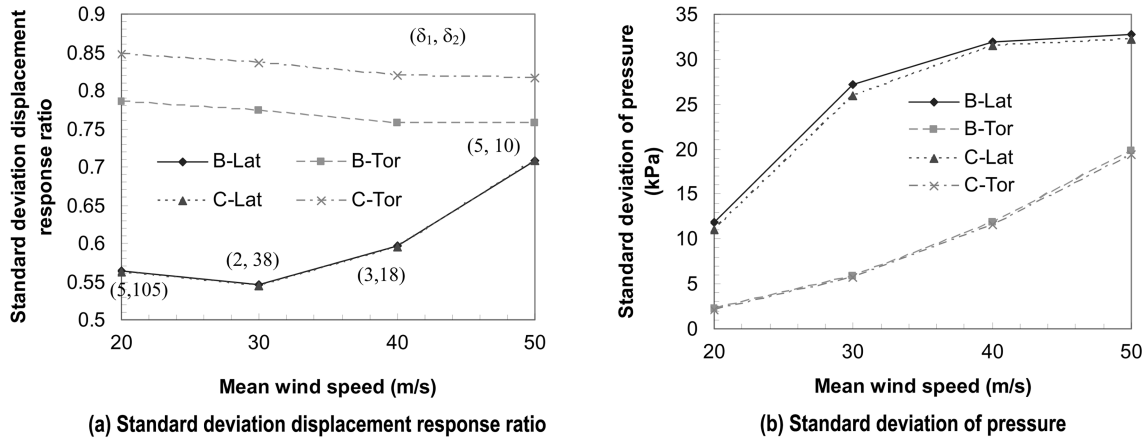


Fig. 11 Effect of mean wind speed

The values inside the parenthesis in Fig. 11 represent the corresponding optimum head loss coefficient. It shows that the standard deviation displacement responses are reduced effectively by the SATLCD. The reduction of lateral displacement by SATLCD is almost at the same level for the mean wind speed of 20 m/s and 30 m/s but it is decreased at the mean wind speed of 40 m/s and 50 m/s. With the inclusion of the control force  $u_{2k}$ , the optimal head loss coefficient of the SATLCD tuned to the lateral frequency of the bridge is increased as the mean wind speed is increased and the maximum value of liquid displacement is found to be about 3.37 m. Since the liquid displacement is controlled within the tolerable limit at high mean wind speed, the energy dissipation which mainly depends on the liquid displacement is thus smaller. Consequently, the reduction of displacement response is smaller. This kind of restriction is also commonly found in the application of other dampers such as tuned mass damper. The maximum stroke of the mass block is always limited by the actual space available inside the structure. Therefore, in some circumstances, the vibration reduction achieved by mass damper at higher wind speed would also be less effective as the stroke of damper is restricted. It is found that the control force  $u_{2k}$  becomes active when the mean wind speed is larger than or equal to 40 m/s.

For the reduction of torsional displacement response, the performance of SATLCD is slightly better as the mean wind speed is increased. The reduction of lateral displacement at points B and C are almost the same while the reduction of torsional displacement at point B is better than that at point C. With the increasing mean wind speed, the optimum head loss coefficient of SATLCD tuned to torsional frequency is decreased but under the influence of the additional damping force, the optimum head loss coefficient of SATLCD tuned to lateral frequency is increased with the increasing mean wind speed. The liquid displacement is controlled within the tolerable limit and therefore the standard deviation of pressure inside the SATLCD tuned to lateral frequency is almost the same at the mean wind speed of 40 m/s and 50 m/s. Figs. 12 and 13 show the time histories of deck displacement at point B together with the pressure inside the SATLCD at point B under the mean wind speed of 20 m/s. Clearly, the pressure inside the SATLCD tuned to the lateral frequency of the bridge varies at a lower frequency and with larger amplitude as compared with that tuned to the torsional frequency of the bridge. There is no vibration reduction in the vertical direction, as expected.

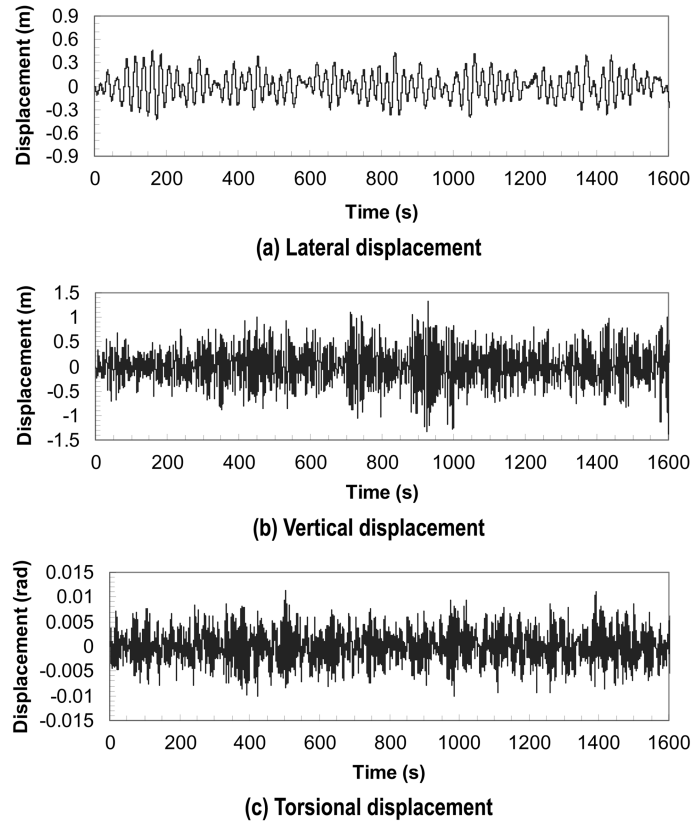


Fig. 12 Time histories of displacements of the bridge with control at point B under construction stage 5 ( $U_m = 20.0$  m/s)

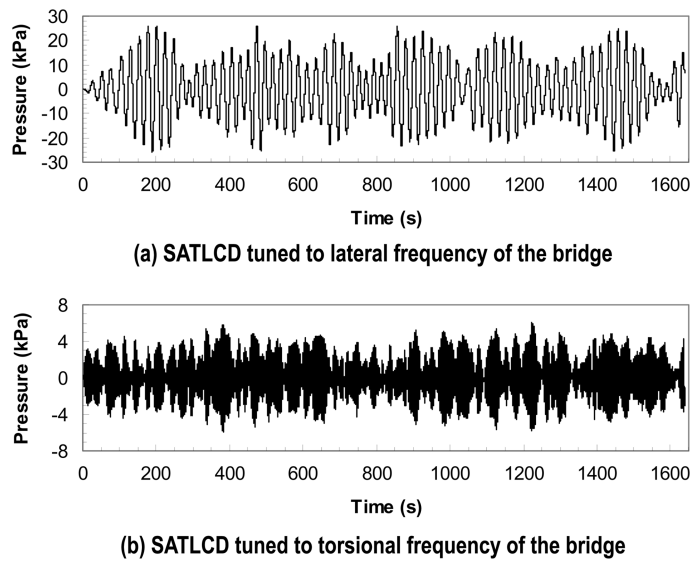


Fig. 13 Time histories of pressure inside SATLCD at point B under construction stage 5 ( $U_m = 20.0$  m/s)

Table 4 Standard deviation of deck displacement with and without control

Location	Lateral (m)		Vertical (m)		Torsional (rad)	
	B	C	B	C	B	C
w/o control ( $U_m=20$ m/s)	0.29746	0.29755	0.37318	0.37437	0.004041	0.003652
With control ( $U_m=20$ m/s)	0.16782 (-43.6%)	0.16739 (-43.7%)	0.37243 (-0.2%)	0.37459 (0.06%)	0.003176 (-21.4%)	0.003094 (-15.3%)
w/o control ( $U_m=50$ m/s)	1.87074	1.87170	2.45735	2.46240	0.031593	0.029666
With control ( $U_m=50$ m/s)	1.32582 (-29.1%)	1.32442 (-29.2%)	2.44805 (-0.38%)	2.45722 (-0.21%)	0.023934 (-24.2%)	0.024204 (-18.4%)

Table 5 Standard deviation of deck acceleration with and without control

Location	Lateral ( $m/s^2$ )		Vertical ( $m/s^2$ )		Torsional ( $rad/s^2$ )	
	B	C	B	C	B	C
w/o control ( $U_m=20$ m/s)	0.05392	0.05410	0.42710	0.41693	0.012370	0.011126
With control ( $U_m=20$ m/s)	0.04027 (-25.3%)	0.04049 (-25.2%)	0.41139 (-3.68%)	0.40715 (-2.35%)	0.009073 (-26.6%)	0.008924 (-19.8%)
w/o control ( $U_m=50$ m/s)	0.42718	0.42861	3.12393	3.05544	0.101623	0.095820
With control ( $U_m=50$ m/s)	0.34159 (-20.0%)	0.34373 (-19.8%)	3.00655 (-3.76%)	2.96235 (-3.05%)	0.077574 (-23.7%)	0.078167 (-18.4%)

The performance of SATLCD is further examined by studying the double deck displacement and acceleration at points B and C. The results for the mean wind speeds at 20 m/s and 50 m/s are tabulated in Tables 4 and 5. It can be seen from Tables 4 and 5 that both the standard deviation displacement and acceleration responses in either lateral or torsional direction are reduced by the SATLCD effectively. The standard deviation displacement reduction in the lateral direction reaches the level of 43% at mean wind speed of 20 m/s and the level of 29% at mean wind speed of 50 m/s. As for the reduction of standard deviation torsional displacement, it can reach the level of 15% at the mean wind speed of 20 m/s and the level of 18% at the mean wind speed of 50 m/s. The standard deviations of lateral, vertical and torsional displacement responses of the bridge deck along the bridge longitudinal axis at the mean wind speed of 20 m/s are plotted in Fig. 14. It can be seen that the maximum standard deviation of the displacement response of the bridge deck occurs at the tip of the two cantilevers. The lateral displacement response of the bridge deck in the uncontrolled case is increased linearly with the increasing distance from the central tower but the torsional displacement in the uncontrolled case is fairly small and is increased suddenly near the tip of the cantilever. This may imply that the torsional stiffness of the deck near the tip of the cantilever is smaller. The lateral displacement response of the whole bridge deck is reduced effectively by the SATLCD. However, for the reduction of torsional displacement, only the part with significant torsional vibration can be reduced.

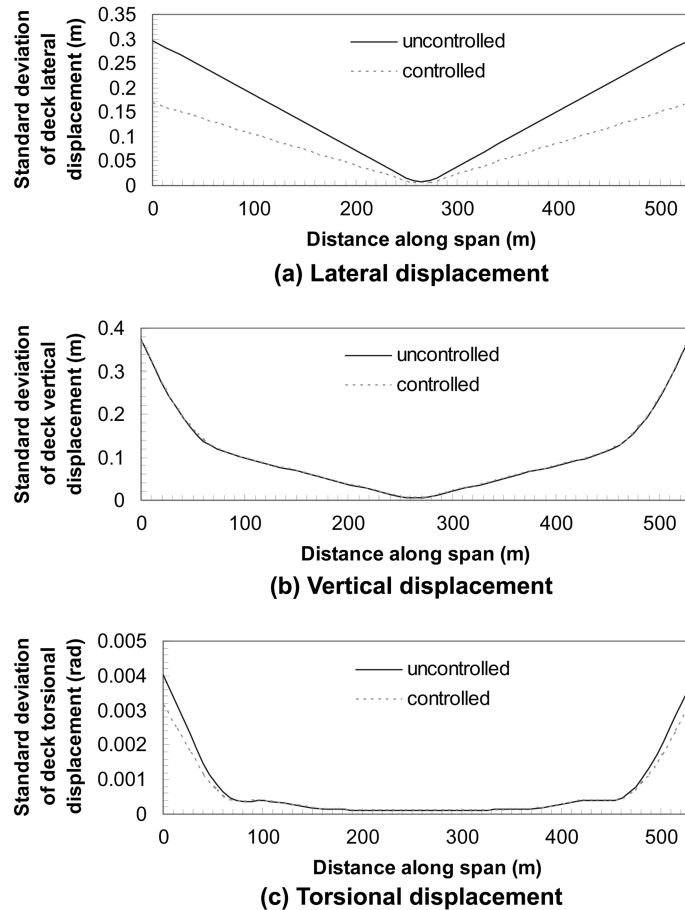


Fig. 14 Standard deviation of deck displacement of the bridge under construction stage 5

#### 6.4. Effect of cantilever length

One of the problems to apply passive liquid column dampers for the suppression of bridge deck vibration during construction arises from the change of bridge dynamic properties from stage to stage. It has been shown in Tables 1 to 3 that the natural frequencies of the double cantilever are varied with the stage of construction in particular for torsional vibration of the concerned bridge. It is thus difficult to apply passive damper with fixed parameters to mitigate the bridge vibrations. However, the natural frequency of the SATLCD can easily be adjusted to match with the updated structural frequency simply by changing the feedback gain of the liquid column damper. This special feature enables it to become a potential device for the suppression of bridge deck vibration with varying frequency during construction. Furthermore, at the initial stage of construction, the torsional vibration of the double cantilever deck is small because of high torsional deck stiffness. Control of lateral vibration is more important than torsional vibration. All SATLCD units are thus tuned to the lateral frequency of the deck at the first two construction stages in this study.

To have a reasonable assessment of the performance of SATLCD in reducing the buffeting response of the bridge, head loss coefficient is taken as a variable to find its optimal value for

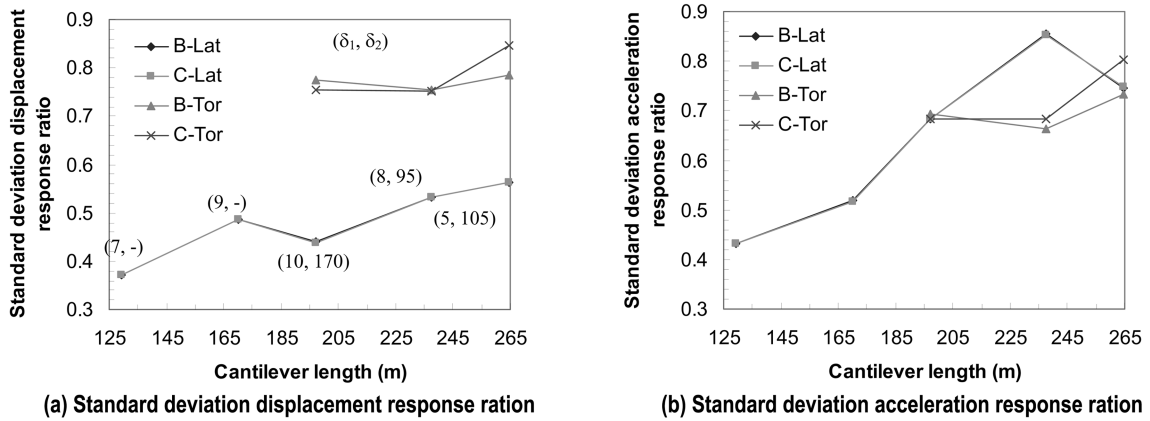


Fig. 15 Effect of cantilever length

achieving the maximum reduction of standard deviation displacement response ratio at each construction stage. Other parameters of the SATLCD used herein are  $H = 6.5$  m,  $\alpha = 0.6$ ,  $\mu = 0.027$ , and  $\mu_L = \mu_T$ . If the structural natural frequency of the bridge deck at each stage is available through field measurement, the frequency of the damper can easily be adjusted to the updated structural natural frequency to maintain high vibration control performance without changing the liquid column length. The reduction of displacement response ratio of the double cantilever deck at the central tower part achieved by the SATLCD units during five different construction stages at a mean wind speed of 20 m/s are plotted in Fig. 15. It can be seen that the performance of SATLCD varies from stage to stage. For the lateral vibration reduction, the performance of SATLCD deteriorates as the cantilever length is increased. For the torsional vibration reduction, the performance of SATLCD is less affected by the increase of the cantilever length when compared with that for lateral vibration reduction. The reduction of lateral vibration obtained by the SATLCD units reaches the level of 40% for standard deviation displacement response and the level of 15% for standard deviation acceleration response ratio. For the torsional vibration, the reduction obtained by the SATLCD units reaches the level of 15% for standard deviation displacement response and the level of 20% for standard deviation acceleration response ratio.

## 7. Conclusions

Semi-active tuned liquid column dampers (SATLCD) have been investigated for the mitigation of wind-induced lateral and torsional vibration of a real long span cable-stayed bridge during five construction stages. The SATLCD can provide a great flexibility for selecting liquid column length while keeping a proper frequency tuning through the change of air pressure acting on liquid. Another feature of the SATLCD is its adaptability to the variation of the bridge frequency under various construction stages. If the updated structural natural frequency of the bridge deck at each stage is available through field measurement, the frequency of the damper can be actively adjusted to the updated structural natural frequency to maintain high vibration control performance. A finite element model of SATLCD was developed in this paper and incorporated into the finite element model of a long span cable-stayed bridge for predicting the buffeting response in the time domain. Extensive parametric studies on SATLCD for the mitigation of wind-induced lateral and torsional

responses of a real long span cable-stayed bridge during construction were carried out in terms of the mass ratio, head loss coefficient, mean wind speed, and cantilever length. The results demonstrated that SATLCD can effectively reduce the lateral and torsional buffeting responses of the cable-stayed bridge. There exists an optimal head loss coefficient for the maximum reduction in either lateral or torsional displacement response. The optimal head loss coefficient for achieving the maximum reduction in lateral displacement is much smaller than that for achieving the maximum reduction in torsional displacement. Both the standard deviation displacement and acceleration responses are reduced effectively by the SATLCD under a wide range of mean wind speeds. The reduction of lateral displacement response by the SATLCD is almost at the same level with the mean wind speed at 20 m/s and 30 m/s but it is decreased at the mean wind speed of 40 m/s and 50 m/s. For the reduction of torsional displacement response, the performance of the SATLCD is slightly better as the mean wind speed is increased. It was also found that with a fixed value of liquid column length, the SATLCD with frequency adaptability can effectively reduce the buffeting response of the bridge deck for all five different construction stages. Since a long span cable-stayed bridge under construction may flutter at low wind speed, the potential performance of SATLCD on increasing the flutter wind speed of the bridge deserves further investigation.

## Acknowledgements

The writers wish to acknowledge the financial support from the Hong Kong Polytechnic University through a PhD studentship to the first writer and through its Area Strategic Development Programme in Structural Control to the second writer.

## References

- Cao, Y.H., Xiang, H.F., and Zhou, Y. (2000), "Simulation of stochastic wind velocity field on long span bridges", *J. Eng. Mech.*, ASCE, **126**(1), 1-6.
- Chen, X.Z., Matsumoto, M., and Kareem, A. (2000), "Time domain flutter and buffeting response analysis of bridges", *J. Eng. Mech.*, ASCE, **126**(1), 7-16.
- Choi, E.C.C. and Brownjohn, J. (1998), "Report on wind tunnel study on the aerodynamic derivatives of the Ting Kau Bridge", Nanyang Technological University, Singapore.
- Conti, E., Grillaud, G., Jacob, J., and Cohen, N. (1996), "Wind effects on the normandie cable-stayed bridge: comparison between full aeroelastic model tests and quasi-steady analytical approach", *J. Wind Eng. Ind. Aerodyn.*, **65**(1-3), 189-201.
- Jelali, M. and Kroll, A. (2003), *Hydraulic Servo-systems: Modelling, Identification and Control*, New York, Springer.
- Kagawa, K., Koukawa, H., Fujita, K., Zensho, Y., and Matsuo, M. (1989), "Development of tuned liquid damper for ship vibration", *Transactions of the West-Japan Society of Naval Architects*, **78**, 251-258.
- Lin, Y.K. and Yang, J.N. (1983), "Multimode bridge response to wind excitation", *J. Eng. Mech.*, ASCE, **109**(2), 586-603.
- Scanlan, R.H. (1978), "The action of flexible bridges under wind. Part 2: Buffeting theory", *J. Sound Vib.*, **60**(2), 201-211.
- Shinozuka, M. and Jan, C.M. (1972), "Digital simulation of random process and its applications", *J. Sound Vib.*, **25**(10), 111-128.
- Shum, K.M. and Xu, Y.L. (2005), "Tuned liquid column dampers with adaptive tuning capacity for structural vibration control", *Struct. Eng. Mech.*, **20**(5), 543-558.
- Takeda, H., Niihara, Y., Ohshio, M., Nakano, R., Kozuma, F., and Ogawa, A. (1998), "Vertical gust response control of long span cable-stayed bridge under cantilever construction by active mass damper", *Proceedings of*

- the 2<sup>nd</sup> World Conference on Structural Control*, pp.835-842.
- Tan, X.M. (1999), "Wind-induced vibration analysis in time domain for long span cable-stayed bridge-engineering application in Hong Kong Ting Kau cable-stayed bridge", Ph.D. Thesis, South China University of Technology, GuangZhou, P.R., China.
- Virlogeux, M. (1992), "Wind design and analysis for the Normandy Bridge", In Larsen A., eds., *Proceedings of the First International Symposium Aerodynamics of Large Bridges*, Copenhagen, Denmark.
- Xu, Y.L., Ko, J.M., and Zhang, W.S. (1997), "Vibration studies of Tsing Ma suspension bridge", *J. Bridge Eng.*, ASCE, **2**(4), 149-156.
- Yang, J.N. (1972), "Simulation of random envelop processes", *J. Sound Vib.*, **21**(1), 73-85.
- Yang, J.N. (1973), "On the normality and accuracy of simulated random processes", *J. Sound Vib.*, **26**(3), 417-428.

CC